ISSN-1996-918X

Pak. J. Anal. Environ. Chem. Vol. 26, No. 2 (2025) 194 – 208

http://doi.org/10.21743/pjaec/2025.12.03

Enhanced Adsorptive and Photocatalytic Degradation of Synthetic Melanoidin Using Silver-Doped TiO_2 Nanoparticles

Mehwish Qaseem[1], Saeed Ahmad[2], Muhammad Yasir Khan[1]*, M. Wasim Akhtar[3], Muhammad Furqan Ali[1], Muhammad Saquib Ali[1], Shakeel Ahmed[1], Shahid Bhutto[4] and Mehwish Altaf[1]

[1]*Department of Chemical Engineering, University of Karachi, Karachi, Pakistan.*
[2]*Department of Chemical Skills, Yanbu Technical Institute, Yanbu, Saudi Arabia*
[3]*Department of Metallurgy & Material Engineering, Mehran University of Engineering & Technology, Jamshoro, Pakistan.*
[4]*Center of Environmental Studies, Pakistan Council of Scientific & Industrial Research (PCSIR), Karachi Complex, Karachi, Pakistan.*
*Corresponding author Email:myasir@uok.edu.pk

Received 22 August 2025, Revised 11 December 2025, Accepted 15 December 2025
Academic Editors: Aamna Balouch and Sarfaraz Ahmed Mahesar

Abstract

Herein, silver-doped titanium dioxide nanoparticles (Ag-TiO_2 NPs) were synthesized via a solution based sol-gel method followed by calcination at 450 °C for 2 h and were utilized in the treatment of synthetic melanoidin solution (SMS). The structural and morphological characterization, conducted through X-ray diffraction (XRD), scanning electron microscopy (SEM) with energy dispersive X-ray spectroscopy (EDX), Fourier-transform infrared spectroscopy (FTIR), and Ultraviolet-visible (UV–Vis) spectroscopy, confirmed the successful integration of silver within the TiO_2 matrix. Ag-TiO_2 NPs showed improved physicochemical properties, such as a reduced band gap of 2.8 eV, as compared to undoped TiO_2. When exposed to visible light (λ > 400 nm), Ag-TiO_2 NPs decolorized SMS by more than 85% in 180 min at pH 7 and an initial melanoidin concentration of 200 mg/L. Also, chemical oxygen demand (COD) and total organic carbon (TOC) were significantly reduced to 60% and 40%. The conversion of recalcitrant melanoidin into more biodegradable byproducts was confirmed by the significant improvement in the biodegradability index (BOD_5/COD) from 0.1 to 0.3. The stability of the catalyst was confirmed through reusability testing, color removal efficiency ranged between 85% to 75% after five cycles. According to kinetic studies, the principal mechanism of degradation is surface-mediated melanoidin adsorption followed by plasmon-induced charge separation, which promotes the production of reactive oxygen species and preserves catalytic performance by lowering surface fouling. Collectively, these findings underscore Ag-TiO_2 NPs as a robust, reusable, and ecologically sustainable solute ion for large-scale melanoidin-rich industrial effluents.

Keywords: Silver-doped TiO_2 nanoparticles (Ag-TiO_2 NPs), Synthetic melanoidin solution (SMS), Visible-light photocatalysis, Photocatalytic degradation

Introduction

Industrial sectors such as distilleries and sugar mills generate significant amounts of colored wastewater that threaten environmental health. Distilleries processing sugarcane or molasses produce molasses spent wash (MSW), a dark-brown, acidic byproduct with high concentrations of organic and inorganic materials [1]. The melanoidin pigments in this effluent block sunlight and reduce dissolved oxygen (DO), harming aquatic ecosystems [2,3]. Traditional biological and physico-chemical treatments often fail to effectively decolourize these waste streams, prompting the search for more effective remediation techniques [4]. Heterogeneous photocatalysis has emerged as a viable solution for degrading stubborn organic pollutants in water [4]. Heterogeneous photocatalysis has emerged as a viable solution for degrading stubborn organic pollutants in water [5]. TiO_2 is a prevalent semiconductor catalyst noted for its oxidizing capability, stability, affordability, and non-toxicity, capable of mineralizing organic compounds under UV light [6]. However, its large bandgap (~3.2 eV for anatase) limits its activation to UV light and causes rapid recombination of photogenerated electron-hole pairs, reducing efficiency under visible light [7]. Enhancing the sensitivity of TiO_2 NPs to visible light and improving charge separation is crucial for their photocatalytic performance against colored compounds. Incorporating silver into TiO_2 (Ag-TiO_2 NPs) addresses these issues, with silver nanoparticles possessing visible-spectrum absorption and forming Schottky junctions that act as electron sinks [8]. This method increases photocatalytic activity to visible light by capturing electrons and inhibiting recombination. Research by Nur et al. has shown notable improvements in the degradation of Acid Red 88 utilizing TiO_2 NPs generated from sol-gel or photo deposition techniques, indicating that doped TiO_2 NPs achieve higher dye degradation rates than undoped TiO_2 NPs [9]. Silver promotes charge separation, enhancing photocatalytic performance, and Ag-TiO_2 NPs also display antimicrobial properties for wastewater disinfection [10]. The nanoscale size of Ag-TiO_2 NPs increases the specific surface area and the number of active sites for the adsorption and degradation of organic compounds [11]. Ag-doped TiO_2 nanostructures have demonstrated remarkable efficacy in adsorbing and photocatalytically degrading several organic pollutants, including dyes, phenolic compounds, and pharmaceutical effluents, according to previous investigations [12,13,14]. Despite its potential, few studies have examined the adsorptive removal of melanoidin using Ag-doped TiO_2 nanomaterials. In addition, published research also falls short in the detail of its equilibrium and kinetic studies. These shortcomings need to be addressed to develop systematic research to comprehend the degradation mechanism of melanoidin by Ag-TiO_2 NPs and to design effective treatment plans. This research investigates the synthesis of Ag-TiO_2 NPs using a sol–gel approach. Fig. 1 provides a detailed schematic diagram outlining the study's overall scope. It also characterizes their structural and optical properties using XRD, UV-Vis spectroscopy, and FTIR spectroscopy. In addition, particle morphology is examined using SEM. The column experiments focus on SMS decolourization. In addition, COD and TOC reductions alongside kinetics to measure the removal efficacy and rate of colour removal, which the Ag-TiO_2 NPs achieve.

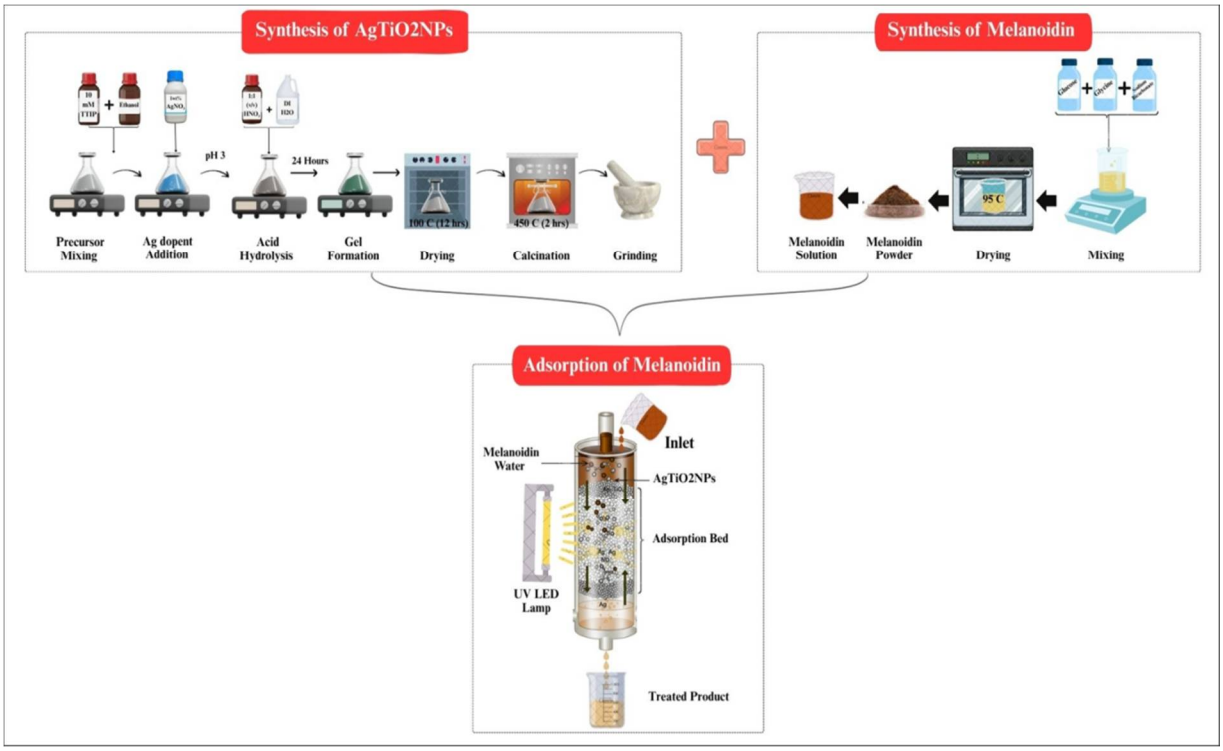

Figure 1: ***Synthesis of Ag-TiO$_2$ NPs / Formation of SMS/adsorption process of SMS***

Materials and Methods

Chemicals and Reagents

The chemical precursors included titanium (IV) isopropoxide (TTIP, ≥97%, Sigma-Aldrich,St.Louis,USA), silver nitrate ($AgNO_3$, ≥99.8%, Merck,Dranstadt, Germany), absolute ethanol (C_2H_5OH, 99.9%, Merck,Germany), and concentrated nitric acid (HNO_3, 69% w/w, Merck,Germany). In order to avoid contamination and ensure reproducibility, all reagents were used without further purification, which may have altered their quality. TTIP was used as the primary titanium source, and silver nitrate was used as the silver dopant. Ethanol was used as a solvent to obtain uniformity in the hydrolysis and condensation processes. To maintain the acidic environment necessary to control hydrolysis and sol-gel network formation, nitric acid was added. For controlled hydrolysis of TTIP during nanoparticle synthesis, distilled Milli-Q water (18.2 MΩ•cm) was used.

Synthesis of Ag-TiO$_2$NPs

A solution of 10 mM TTIP was prepared in 50 mL of absolute ethanol, stirred at 500 revolutions per minute in a nitrogen chamber to prevent unwanted hydrolysis. A silver nitrate ($AgNO_3$) component, 1 wt% relative to TiO_2 (0.1 g per 10 g of TiO_2), was added and stirred for 30 min for Ag^+ ion distribution. Hydrolysis was initiated by dropwise addition of a 1:1 (v/v) HNO_3-Milli-Q water solution, maintaining the pH at 3 to control sol-gel kinetics [15]. The solution was aged for 24 h at 25 °C, forming a translucent gel, which was dried at 100 °C for 12 h to create a porous xerogel. This xerogel was ground and calcined at 450 °C for 2 h (5 °C min^{-1} ramp rate), resulting in crystalline anatase TiO_2 and reducing Ag^+ to metallic silver nanoparticles. A control TiO_2 sample was also synthesized without $AgNO_3$ under the same conditions.

Characterization

The structural characteristics of nanoparticles were examined using X-ray diffraction (XRD, Bruker D8 Advance,Germany) with Cu Kα radiation (λ = 1.5406 Å) and a current of 200 mA. All data from 20° to 80° in the XRD spectrum were integrated and recorded, and the characteristic peaks were determined by comparison with the Joint Committee on Powder Diffraction Standards. Morphology and elemental composition were analyzed using field-emission scanning electron microscopy (FE-SEM, JEOL JSM-7100F, Japan) and energy-dispersive X-ray spectroscopy (EDS) at 15 kV. Optical absorption properties were evaluated by UV–Vis diffuse reflectance spectroscopy (DRS; Shimadzu UV-2600, Japan), with band gaps determined from Tauc plots of Kubelka–Munk data. BOD_5 and COD of the samples were analyzed and assessed according to pertinent incubation and titration methods over 5 days, using closed reflux with $K_2Cr_2O_7$ in sulfuric acid, respectively, as outlined in the literature [16]. Each experiment was repeated three times, and the SEM and XRD apparatus were calibrated using a gold-coated silicon wafer and a Si standard, respectively.

Preparation of SMS

Bernado et al. (1997) used glycine, sodium carbonate, and glucose to stimulate SMS [17]. They measured 0.42 g of sodium carbonate, 1.88 g of glycine, and 4.5 g of glucose. These were diluted with 100 millilitres of distilled water, and the mixture was kept in the oven at 95 °C for 7 h. Freeze-drying at -30°C to -40°C at vacuum (1 torr) was done once the fluid attained room temperature. The melanoidin generated by this mechanism had a molecular weight of 10,000-15,000 Da.

Fixed-Bed Column Setup

A glass column setup was established to separate packed Ag-TiO_2 NPs and undoped TiO_2 NPs, with a length of 30 cm and an inner diameter of 1.5 cm. To alleviate voids and channelling effects, the packing was carefully tapped, and the parameters for bed height and adsorbent mass were carefully controlled [18]. The column was flushed with distilled water to ensure the stability of the packed bed. To enable both adsorption and photocatalytic decolourization tests, SMS was added to the system under controlled flow conditions.

Continuous Flow Adsorption/ Degradation Experiments

Fixed-bed column experiments were conducted under continuous flow to analyze melanoidin adsorption and photocatalytic degradation efficiency. The influent solution was directed through a catalyst bed using gravitational flow, with bed heights of 2 cm, 5 cm, and 8 cm and a fixed internal diameter of 1.5 cm. Flow rates were set at 1, 2, and 4 $mLmin^{-1}$. For degradation experiments, the influent pH was adjusted to 3, 5, 7, or 9 using HCl or NaOH [19]. The initial melanoidin concentrations of 100, 200, 500, and 800 mgL^{-1} were selected [20]. The catalyst dosage was changed from 1.5, 3 and 4.5 gL^{-1}. The two catalyst systems were used: undoped TiO_2 NPs and Ag-TiO_2 NPs, under visible LED irradiation at (λ > 400 nm, 50 mW cm^{-2}, 30 W) and in the dark. SMS samples were placed for breakthrough analysis and degradation efficiency assessment. The percentage removal of melanoidin was calculated using equation (1):

$$\%\, removal = \frac{C_o - C_t}{C_o} \times 100 \qquad (1)$$

Where C_o represents the initial concentration of the melanoidin solution, and C_t represents the concentration at a specific irradiation time, *t* [21].

Results and Discussion

SEM (Morphology) analysis of Ag-TiO_2 NPs

According to SEM images (Fig. 2A), Ag-TiO_2 NPs exhibit a predominantly spherical nanoscale morphology. It can be seen from Fig. 2A (a-c). The strong interparticle interactions and high surface energy of oxide nanostructures lead to localized agglomeration [22]. The detached clusters are an appropriate arrangement for both adsorption and catalytic activities. In Fig. 2A (d), EDS analysis has confirmed the presence of uniformly distributed titanium, oxygen, and silver. The lack of redundant peaks indicates that there are no observable contaminants or later stages from the synthesis process [23]. As demonstrated in Fig. 2B (a-e), elemental mapping investigations were performed to confirm silver incorporation inside the TiO_2 matrix. Silver was embedded in the matrix and effectively integrated into the TiO_2 lattice, as evidenced by the overlap of silver signals with the TiO_2 areas [24]. In order to improve visible light absorption and decrease charge recombination, Ag must be evenly scattered throughout the TiO_2 matrix.

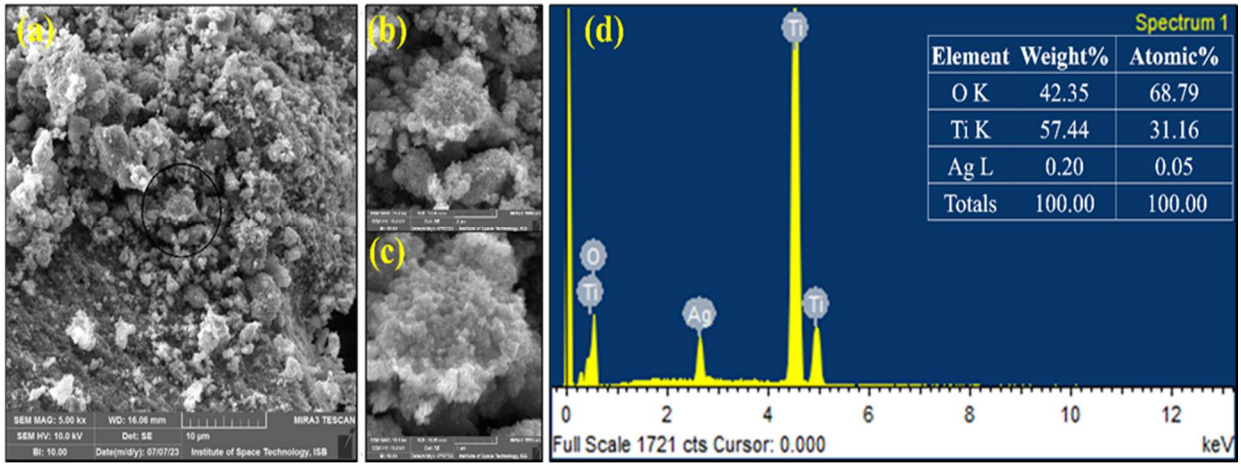

Figure 2A. SEM analysis of Ag-TiO_2 NPs, (a) 5.0 kx, (b) 25 kx, (c) 50 kx, (d) EDS spectrum of Ag-TiO_2 NPs

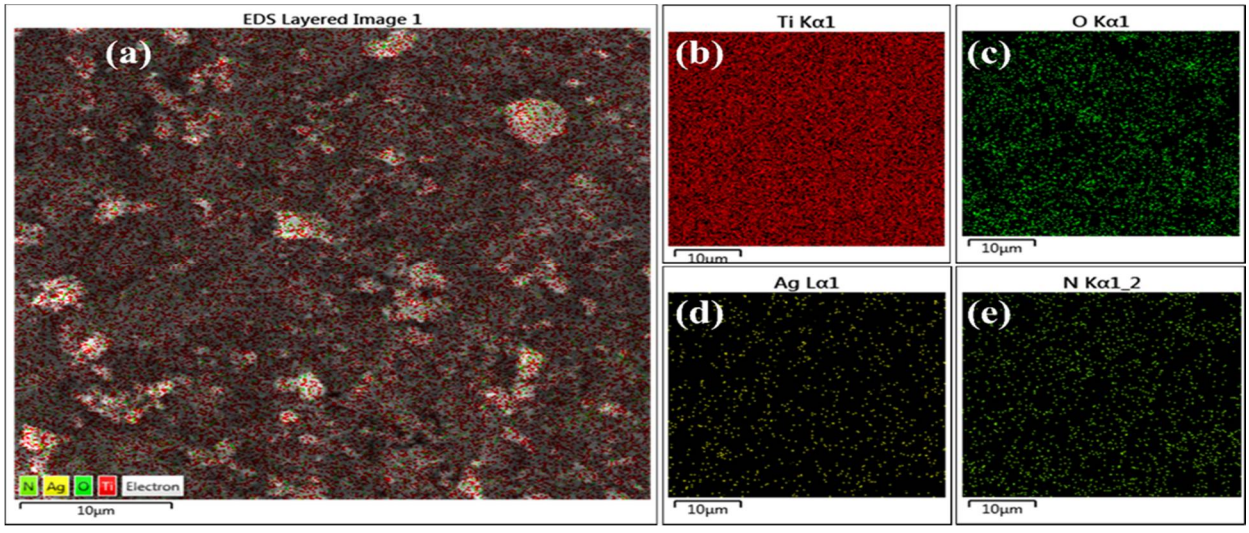

Figure 2B. Elemental mapping of Ag-TiO_2 NPs, (a) Overall image, (b)Ti, (c) O, (d) Ag, (e) N

XRD analysis of Ag-TiO_2 NPs

According to XRD analysis, the synthesized Ag-TiO_2 NPs predominantly exhibited an anatase phase, as shown in Fig. 3a. The JCPDS 21-1272 database identifies distinct peaks at approximately 25.3° (101), 37.8° (004), 48.0° (200), 54.0° (105), and 62.7° (204) [25]. The well-formed crystal structures of the as-prepared TiO_2 are indicated by the clear, sharp diffraction peaks and the absence of any additional impurity peaks.

The dearth of rutile, elemental Ag, or Ag_2O peaks indicates that silver is either integrated into or distributed across the TiO_2 lattice. Ag-TiO_2 NPs showed a modest shift in diffraction peaks and a broadening of peaks in comparison to undoped TiO_2 NPs, suggesting potential lattice deformation from silver incorporation [26]. According to the Scherrer equation (eq 2), the particle size is estimated to be ~ 17 nm. The findings show that Ag doping improves structural properties that are advantageous for better adsorption and photocatalytic performance while inhibiting grain expansion [27].

$$D = \frac{K\lambda}{\beta cos\,\theta} \quad (2)$$

FTIR analysis of Ag-TiO_2 NPs

Undoped TiO_2NPs and Ag-TiO_2NPs show notable structural alterations as a result of silver incorporation in their FTIR spectra. It is evident from Fig. 3b that, spectrum of undoped TiO_2 NPs has a large absorption band at around 3400 cm^{-1} and a smaller band near 1630 cm^{-1}, which are indicative of surface water-related hydroxyl group vibrations. Below 1000 cm^{-1}, Ti–O lattice vibrations are noted [28]. However, the introduction of silver leads to marked spectral alterations, with slight shifts and intensity changes in the Ti–O vibrational modes, indicating disruptions in local bonding due to the presence of the silver ion. Significantly, decreased hydroxyl group binding on the silver-modified surface is implied by intensity reductions in hydroxyl-related bands at roughly 3400 cm^{-1} and 1630 cm^{-1}, indicating altered surface chemistry. These modifications facilitate the efficient incorporation of Ag into the TiO_2 matrix, altering surface states and metal–oxygen interactions, which is essential for increased visible-light photocatalytic activity [29].

UV-Vis Spectra of Ag-TiO_2 NPs

The optical absorption characteristics of undoped TiO_2 NPs and Ag-TiO_2 NPs were investigated using UV-Visible spectroscopy. As shown in Fig. 3c, undoped TiO_2 NPs display strong absorption in the UV region, with an absorption edge corresponding to a bandgap energy of approximately 3.26 eV, indicative of the anatase phase. However, their minimal absorption in the visible range limits photocatalytic efficiency [30]. In contrast, Ag-TiO_2 NPs exhibit a red shift of the absorption edge to 360 nm, enabling enhanced visible region absorption. This shift arises from silver doping, which promotes localized surface plasmon resonance (LSPR) and alters the electronic band structure [31], thereby increasing photon capture in the near-UV and visible regions. The inset of Fig. 3c shows that the bandgap of Ag-TiO_2 NPs falls between 2.7 and 2.8 eV, lower than undoped TiO_2 NPs. These results confirm that the optical properties and bandgap of anatase-phase TiO_2 can be significantly modified, enabling efficient visible-light photocatalysis and improved suitability for environmental purification applications [32].

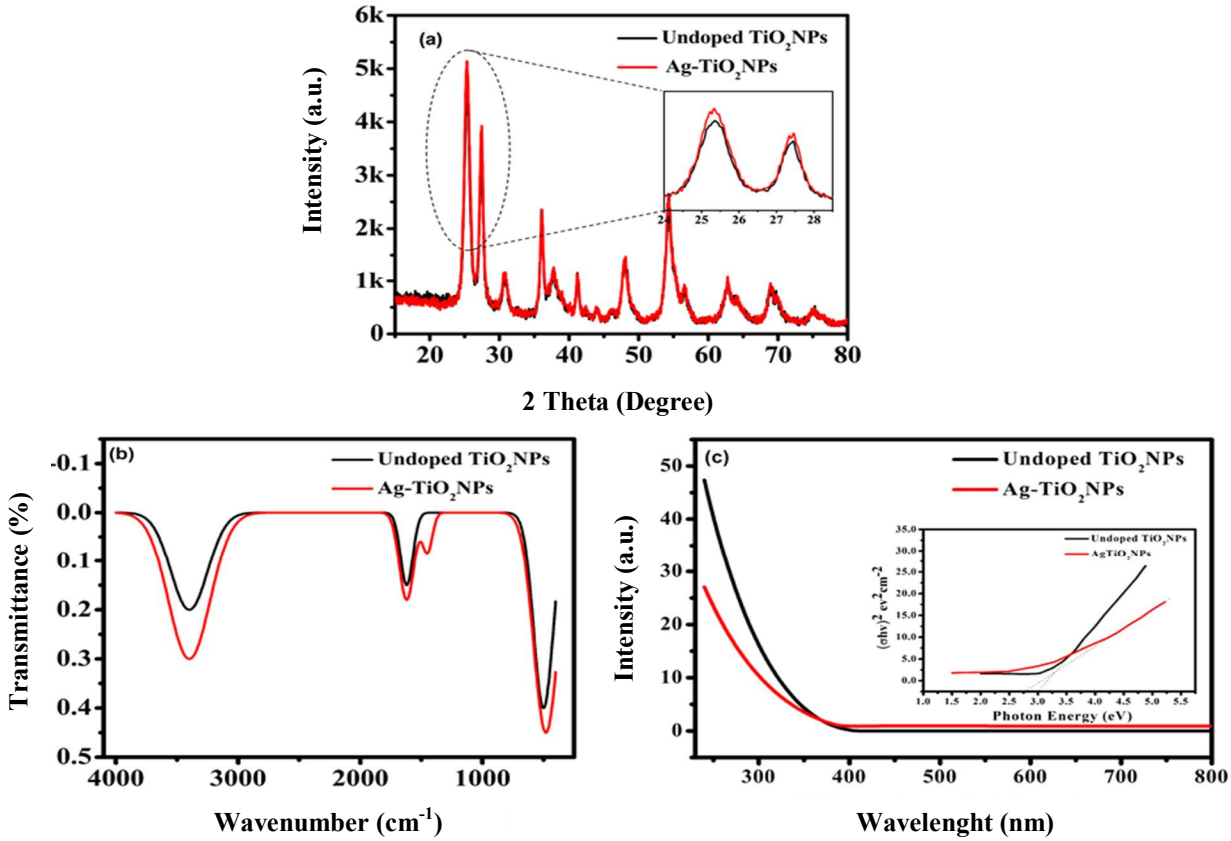

Figure 3. ***(a)*** **XRD analysis of undoped TiO_2 NPs and Ag-TiO_2 NPs (Inset shows close effect of Ag doping on position and intensity of TiO_2 peaks), (b) FTIR analysis of undoped TiO_2 NPs and Ag-TiO_2 NPs, (c) UV-Vis analysis of undoped TiO_2 NPs and Ag-TiO_2 NPs (Inset shows plots of $(\alpha h\nu)^{1/2}$ versus photon energy for the direct band gap energies of undoped TiO_2 NPs and Ag-TiO_2 NPs)**

MS Decolorization Efficiency

The environment in which decolourization occurs depends significantly on the type of catalyst used. As illustrated in Fig. 4, Ag-TiO_2 NPs performed better at decolourisation than undoped TiO_2 NPs. In the absence of light, around 75% of the colour within the 180-min interval was removed using the Ag-TiO_2 NPs catalyst. In comparison, undoped TiO_2 removed only 60% of the colour. In the presence of UV light, Ag-TiO_2 NPs showed a significant increase in decolourisation, reaching nearly 85% within the same period. Under dark conditions, both catalyst types reached a plateau. However, the increase in the Ag-TiO_2 NPs decolourisation curve in the presence of light was more pronounced, approaching complete colour removal. This data suggests that light absorption combined with silver doping photochemically activates Ag-TiO_2 NPs and dramatically improves the catalytic oxidative degradation of SMS [33].

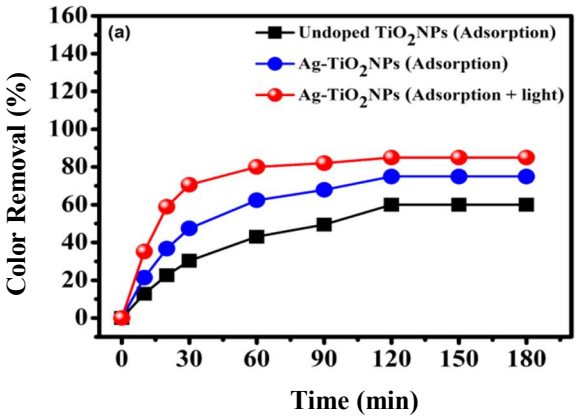

Figure 4. **SMS degradation (% color removal) at various contact time**

UV–Vis spectral analysis of SMS under catalytic treatment

The spectral examination of SMS shows notable differences in photocatalytic efficiency across the tested systems (Fig. 5). The untreated solution strongly absorbs UV light (200–325 nm). It shows a broad, visible peak at 420 nm, which gives it its brown colour. These absorption properties remain stable for 180 min with undoped TiO_2 NPs (Fig. 5a), suggesting that removal is mainly by adsorption rather than degradation. Adding Ag-TiO_2 NPs (Fig. 5b) slightly reduces the UV and visible absorption peaks, suggesting partial breakdown of the melanoidinchromophore without complete mineralization. On the other hand, Ag-Ti_2 NPs subjected to UV radiation (Fig. 5c) show a notable and consistent decline throughout the spectral range, which eventually leads to the 420 nm band being nearly completely obliterated by 180 minutes. According to this phenomenon, a two-step degradation mechanism. Melanoidin molecules first adsorb onto the catalyst surface, followed by photocatalytic oxidation and final mineralization aided by photogenerated charge carriers. The results indicate enhanced decolourization, a significant reduction in TOC, and increased effluent biodegradability. This evidence suggests a synergistic adsorption and plasmon-assisted photocatalysis in the Ag-TiO_2 NPs-based process [34].

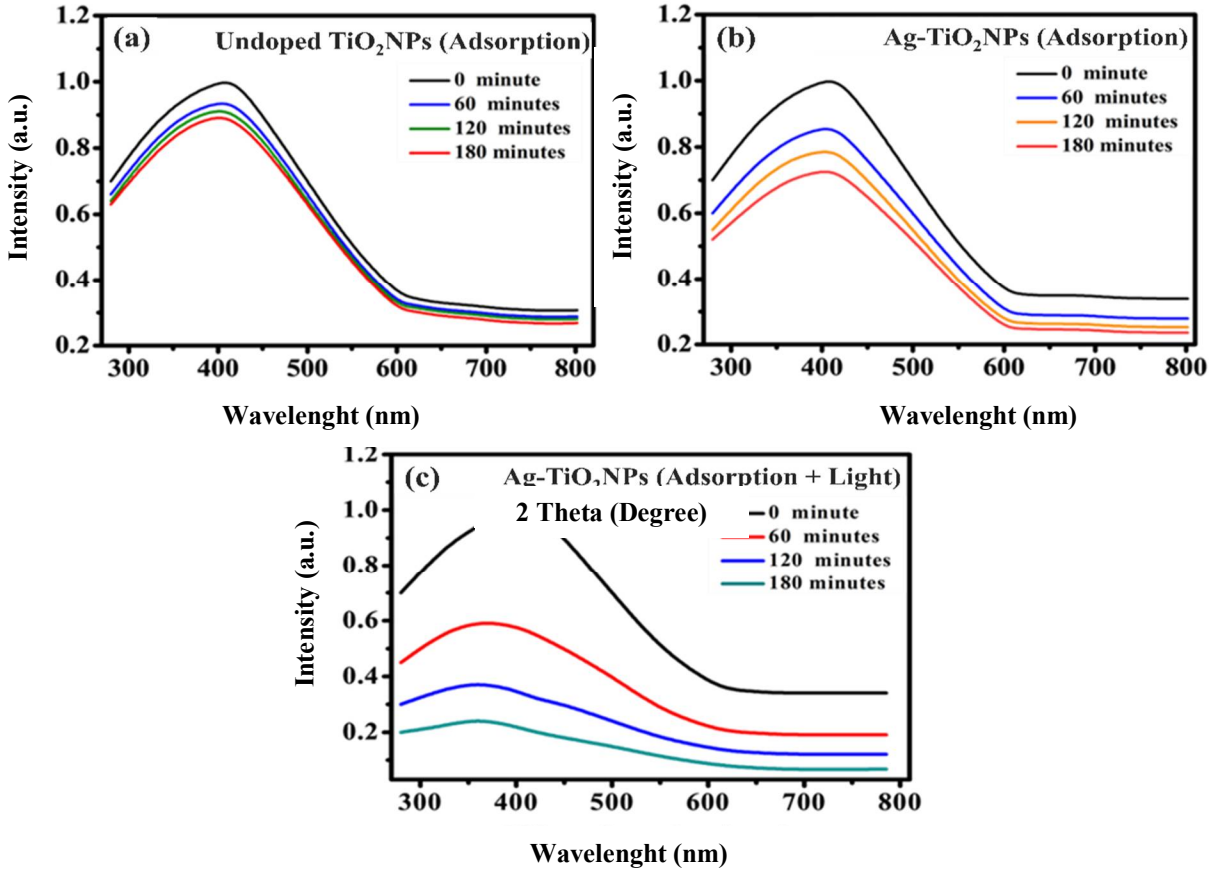

Figure 5. **The UV–Vis spectral analysis of SMS undergoing catalytic treatment. Time-resolved analysis of (a) undoped TiO_2 NPs), (b) Ag-TiO_2 NPs, and (c) Ag-TiO_2 NPs with light**

Mineralization Indicators of SMS

TOC Remediation: Ag-TiO_2 NPs significantly enhanced SMS treatment beyond colour elimination. Fig. 6a showed a consistent diminution in TOC, with Ag-TiO_2 NPs exposed to light achieving approximately 40% reduction after 180 min, in contrast to about 10% in the dark and roughly 4% for undoped TiO_2. Early on (≤40 min), the kinetics showed a similar trend, demonstrating the rapid effectiveness of Ag-TiO_2 NPs when UV driven. These findings demonstrate the mutually beneficial effects of photoactivation and silver doping, establishing Ag-TiO_2 NPs as a successful photocatalytic method for breaking down organic contaminants [35].

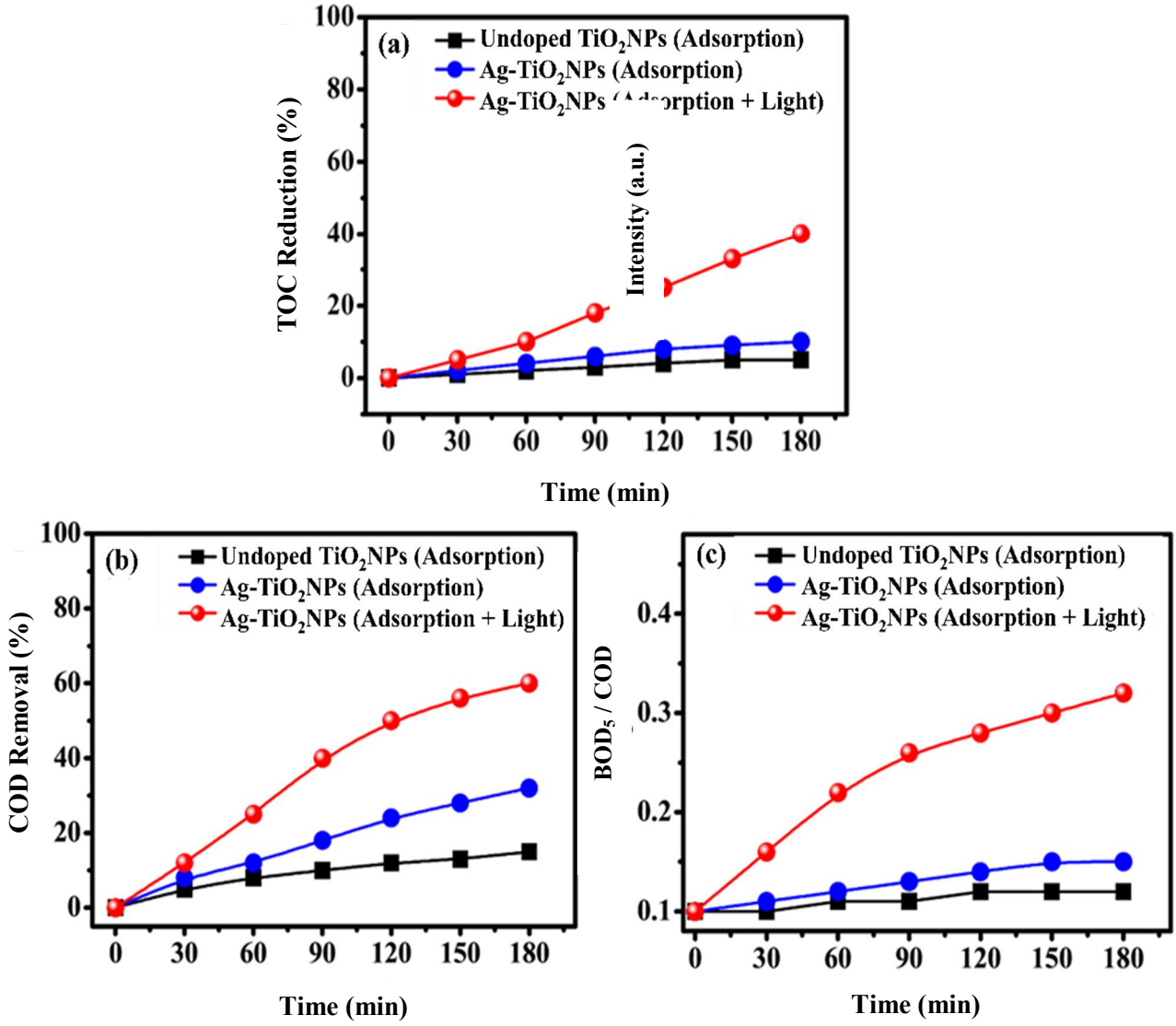

Figure 6(a). **Impact of TOC reduction % of SMS on adsorption, (b) biodegradability analysis includes COD removal and (c) BOD_5/COD ratio) of SMS absorbed over time.**

Biodegradability Improvement (BOD_5/COD Ratio)

In Fig. 6 (b&c), the improvement in biodegradability is noteworthy and indicates a two-step mechanism. First, photocatalytic oxidation breaks down challenging organic molecules into smaller, more easily biodegradable forms. Fig. 6b shows COD removal percentages. Ag-TiO_2 NPs achieve about 60% COD elimination after 180 min of irradiation, the highest observed. Undoped TiO_2 NPs achieve about 15% COD removal. Dark adsorption on Ag-TiO_2 NPs gives around 32% COD removal. Fig. 6c shows the evolution of the BOD_5/COD ratio. All treatments significantly increase the ratio above the raw effluent baseline, which is about 0.1. After 180 min, photocatalysis with Ag-TiO_2 NPs achieves the highest ratio at around 0.30. In comparison, undoped TiO_2 NPs reach about 0.1, and Ag-TiO_2 NPs without light attain around 0.13. This indicates oxidation in the first step makes the second step—biological treatment work better. Thus, Ag-TiO_2 NPs under UV light are the most effective photocatalyst, as this two-step process improves biodegradability and significantly reduces organic load, beyond simple adsorption [36].

Catalyst Reusability and Stability

An effective catalyst must regenerate and maintain performance over multiple cycles, as shown in Fig. 7. Reusability tests show that the color removal efficiency declined to about 75% after five uses from 85% color removal in the first cycle with UV-irradiated Ag-TiO_2 NPs. In dark conditions, Ag-TiO_2 NPs' efficiency dropped from 52% to 46%, while undoped TiO_2 NPs fell from 38% to 33%. Ag-TiO_2 NPs' performance reduction likely results from surface fouling or minor silver leaching, though they remained active. These results highlight Ag-TiO_2 NPs' resilience and practical value in photocatalytic processes [37].

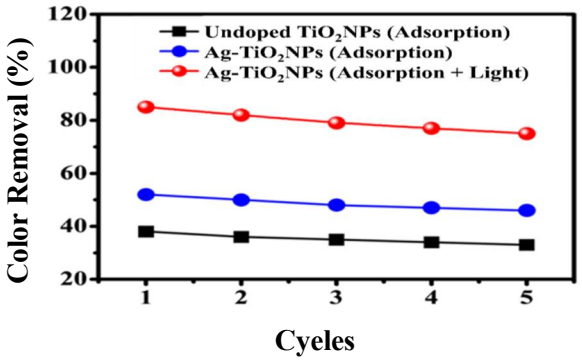

Figure 7. **Reusability and stability of catalysts over five successive cycles**

Kinetics and Degradation Efficiency

Fig. 8 shows the degradation kinetics of SMS, the natural logarithm of the concentration ratio, ln (Co/C). The catalytic systems almost always exhibited a biphasic degradation profile with propulsive degradation. Initially, they removed a higher percentage of the substance, then reached equilibrium. Without a dopant, TiO_2 NPs consistently reached a 60% removal (ln (Co/C) = 0.91) after 180 min.

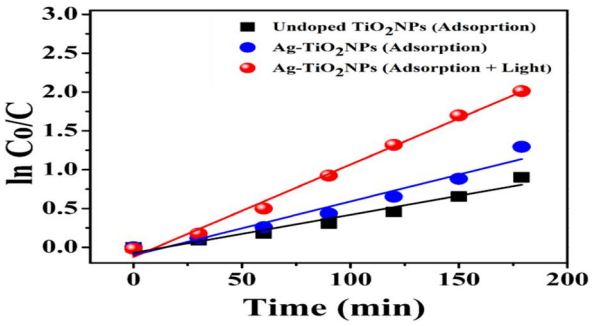

Figure 8. **Degradation kinetics of SMS against natural logarithm of the concentration ratio**

This suggests a weak activity dominated by adsorption. In the dark, Ag-TiO_2 NPs showed ln (Co/C) close to 1.38. In contrast, the Ag-TiO_2 NPs photocatalyst reached ln (Co/C) = 0.92 after 90 min. After 180 min, it achieved roughly 85% elimination

(ln (Co/C) ≈ 1.9). Kinetic research indicates a positive slope in the –ln (C/C$_o$) versus time relationship during the initial stages, consistent with the pseudo-first-order model. Compared with rate constants driven solely by adsorption, the slopes showed higher rates under photocatalytic conditions. This behavior is in line with Langmuir-Hinshelwood kinetics, which states that light promotes the oxidative mineralization of persistent organic molecules. Consequently, the Ag-TiO_2 NPs under the radiation system show improved catalytic lifespan and degradation efficacy compared to both the dark Ag-TiO_2 NPs and undoped TiO_2 NPs systems [38]. The values of the constant for all three conditions were summarized in Table 1.

Table 1. **Kinetic parameters and their constant values under three different conditions.**

Conditions	Linear Equation	K_1x10^{-3} (min^{-1})	R^2
Bare TiO_2	$\ln(C_0/C) = K_1t$	4.0	0.95
Ag-TiO_2 NPs		6.9	0.95
Ag-TiO_2 NPs (Light)		11.8	0.99

Breakthrough Curve Analysis

The dynamic adsorption behavior of SMS over Ag-TiO_2 NPs in a fixed-bed column was assessed using breakthrough experiments that plotted the effluent-to-influent concentration ratio (C_t/C_o) as a function of time for a given bed height and flow rate, yielding an S-shaped breakthrough curve.

Effect of bed height and flow rate

Fig. 9a shows the breakthrough curve for the adsorption of melanoidin at bed heights of 2 cm, 5 cm, and 8 cm, keeping the flow rate [1 mL/min] and initial concentration [200 mg/L] constant. It can be seen from the plot that for a higher bed height of 8 cm, the breakthrough curve displayed relatively fewer steep tendencies, indicating a longer breakthrough time at (Ct/C=0.1) is 80 min. This is due to a greater number of available sites for melanoidin uptake, resulting in a higher adsorption capacity. As the mass transfer zone advanced from the inlet to the outlet of the fixed-bed column, it was observed that both breakthrough time and exhaustion time increased with bed height, as reported in the literature [39]. The effect of flow rate was investigated at 1 mL/min, 2 mL/min and 4 mL/min while keeping the bed height of 5 cm and initial concentration of 200 mg/L constant, as depicted in Fig. 9b. The increase in flow rate decreases the breakthrough time (tb) and bed saturation time (ts). Breakthrough time (10%) was 60 min, 40 min and 30 min for 1 mL/min, 2 mL/min and 4 mL/min, respectively. Both (tb) and (ts) were inversely correlated with the inflow rate; the bed saturates more quickly at higher flow rates than at lower ones because the contact time between the adsorbent and the absorbate decreases [40].

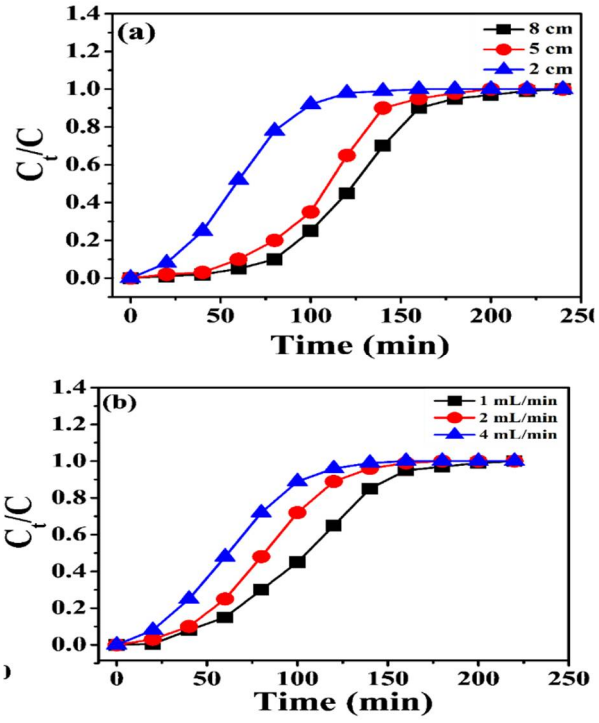

Figure 9. **Breakthrough curve, (a) Effect of bed height (b) Effect of flow rate**

Possible mechanism for SMS photocatalytic degradation by Ag-TiO_2NPs

When the Ag-TiO_2NPs were exposed to radiation, an electron (e) is excited from the valence band (VB) to the conduction band (CB) of TiO_2, leaving a positive hole h+ in the VB. The silver nanoparticles often function as electron sinks or electron traps, due to the creation of a Schottky barrier at the Ag/TiO_2 interface, which efficiently separates the charge carriers and significantly reduces e-/h+ recombination [41]. While the trapped electron on the Ag surface is transported to adsorbed oxygen (O_2) to form the superoxide radical ($O_2^{\cdot-}$), the isolated hole (h+) on the TiO_2 surface combines with adsorbed water or hydroxyl ions (OH-) to produce the potent oxidant, the hydroxyl radical (OH) [42]. Additionally, the catalyst's activity is extended beyond the UV range by metallic Ag nanoparticles, which utilize the Localized Surface Plasmon Resonance (LSPR) phenomenon [43] under visible light to produce and inject "hot" electrons into the TiO_2 CB. The complex, polymerized melanoidin molecules are ultimately chemically attacked by these (OH) and ($O_2^{\cdot-}$) radicals, which cause their breakdown and subsequent mineralization into simple, non-toxic compounds. The mechanism of photocatalytic degradation is depicted in Fig. 10.

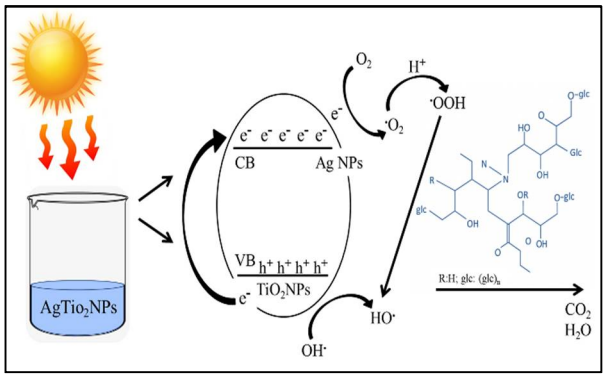

Figure 10. **Photocatalytic degradation mechanism of SMS by Ag-TiO_2 NPs**

Comparison with other adsorbents

Table 2 presents a comparative evaluation of the as-synthesised Ag-TiO_2 NPs with other reported adsorbents for the removal of SMS, including metal oxides and their composites, Cu-impregnated activated carbon, and a polymer-based adsorbent. Adsorbents like activated carbon or metal-impregnated activated carbon have inherent drawbacks, such as waste production, limited reusability, high cost, and sustainability issues. Similarly, the nanocomposite demonstrated an effective removal rate of more than 85%; however, the use of metal oxides in composites renders them expensive and unsuitable for widespread industrial use. Although polymer-based adsorbents such as Rosin-based polymer @ silica core- shell exhibit excellent melanoidin removal efficiency (up to 92%), their low mechanical and thermal stability, as well as the comparatively expensive cost of synthesis, limit their practical use. Unlike the above-mentioned adsorbents, Ag^+ ions and nanoscale dispersion enable Ag-TiO_2 NPs to overcome these limitations by improving electron transmission and pollutant binding affinity, yielding up to 85% melanoidin removal. The catalyst properties and their performance metrics are summarized in Table 3.

Table 2. **Comparative study of various nanoadsorbents for SMS degradation.**

Adsorbent	Removal Efficiency (%)	Optimal pH	Contact Time (min)	Ref
PCAM@HNTs	98.53 %	7	-	4
RP-Si-CA	92%	7	180	45
Cu-impregnated AC	73%	3	-	46
TiO_2-ZnO/AC composite	86%	5	-	47
Ag-TiO_2NPs	85%	7	180	This study

Table 3. **Ag-TiO_2 NPs characteristics, operational parameters and their performance evaluation.**

Catalyst	Catalyst properties		Process parameters		Performance Metrics	
Ag-TiO_2NPs	Band gap (eV)	2.8	pH	7	% color removal	85%
	Structure	Crystal	Adsorbate Conc (mg/l)	200	Biodegradability index	0.30
	Particle size	~17nm	Time (min)	180	Kinetics rate (min^{-1})	0.0118

Conclusion

The synthesized Ag-TiO_2 NPs demonstrated high SMS remediation efficiencies through simultaneous adsorption and photocatalytic degradation. In fixed-bed column experiments, breakthrough time increased with greater bed height and lower flow rate. The biodegradability index (BOD_5/COD) rose from 0.1 to 0.3, indicating the transformation of recalcitrant melanoidin into less toxic, more biodegradable byproducts. Reaction pathways and efficiencies were evaluated using kinetic models, with the rate constant increasing from 0.0027 min^{-1} to 0.0118 min^{-1}. The presence of silver nanoparticles enhanced charge-carrier separation and reduced electron-hole recombination, while visible-light absorption further improved photocatalytic activity. Increased surface area and a greater number of active sites promoted stronger adsorption of melanoidins, resulting in more rapid and complete degradation. Overall, Ag-TiO_2 NPs proved to be both economically viable and environmentally sustainable, achieving significant decolourisation and reductions in organic load in effluents from distillery and sugar factory sources.

Conflict of Interest

The authors declare that they have no conflict of interest.

References

1. P. A. Shinde, T. M. Ukarde, P. H. Pandey and H. S. Pawar, *J. Water Process Eng.,* 36 (2020) 101353. doi:10.1016/j.jwpe.2020.101353
2. R. Chandra, R. N. Bharagava and V. Rai, *Bioresour. Technol.,* 99 (2008) 4648. doi:10.1016/j.biortech.2007.09.057
3. R. Al-Tohamy, S. S. Ali, F. Li, K. M. Okasha, Y. A.-G. Mahmoud, T. Elsamahy, H. Jiao, Y. Fu and J. Sun, *Ecotoxicol. Environ. Saf.,* 231 (2022) 113160. doi:10.1016/j.ecoenv.2021.113160
4. M. Tripathi, S. Singh, S. Pathak, J. Kasaudhan, A. Mishra, S. Bala, D. Garg, R. Singh, P. Singh, P. K. Singh, A. K. Shukla and N. Pathak, *Toxics,* 11 (2023) 940. doi:10.3390/toxics11110940
5. Y. Song, L. Wang, X. Qiang, W. Gu, Z. Ma and G. Wang, *J. Water Process Eng.,* 55 (2023) 104242. doi:10.1016/j.jwpe.2023.104242
6. C. Zarzzeka, J. Goldoni, J. R. de Paula de Oliveira, G. G. Lenzi, M. D. Bagatini and L. M. S. Colpini, *Sustain. Chem. Environ.,* 8 (2024) 100177. doi:10.1016/j.scenv.2024.100177
7. N. M. Chauke, A. Ngqalakwezi and M. Raphulu, *Int. J. Environ. Sci. Technol.,* 22 (2025) 8521. doi:10.1007/s13762-025-06397-2
8. N. Ramesh, C. W. Lai, M. R. B. Johan, S. M. Mousavi, I. A. Badruddin, A. Kumar, G. Sharma and F. Gapsari, *Heliyon,* 10 (2024) e40998. doi:10.1016/j.heliyon.2024.e40998
9. S. M. A. Nur, M. Sultana, A. Mondal, S. Islam, F. N. Robel, A. Islam and M. S. A. Sumi, *J. Water Process Eng.,* 47 (2022) 102728. doi:10.1016/j.jwpe.2022.102728
10. D. Shan, Y. Zhao, L. Liu, X. Linghu, Y. Shu, W. Liu, M. Di, J. Zhang, Z. Chen,

H. Liu and B. Wang, *Environ. Technol. Innov.,* 30 (2023) 103059. doi: 10.1016/j.eti.2023.103059
11. H. Dhila, A. Bhapkar and S. Bhame, *Desalin. Water Treat*., 321 (2025) 101004. doi:10.5004/dwt.2025.101004
12. R. Hidayat, G. Fadillah, S. –I. Ohira, F. I. Fajarwati, D. A. Setyorini and A. Saputra, *Mater. Today Sustain.,* 26 (2024) 100752. doi:10.1016/j.mtsust.2024.100752
13. V. Uthiravel, K. Narayanamurthi, V. Raja, S. Anandhabasker and K. Kuppusamy, *Inorg. Chem. Commun.,* 170 (2024)113327. doi:10.1016/j.inoche.2024.113327.
14. A.A. Assadi, S. Karoui, K. Trabelsi, A. Hajjaji, W. Elfalleh, A. Ghorbal, M. Maghzaoui and A. A. Assadi, *Materials,* 15 (2022) 1463. doi:10.3390/ma15041463.
15. A. Payan, M. Fattahi and B. Roozbehani, *J. Environ. Health Sci. Eng.,* 16 (2018) 41. doi:10.1007/s40201-018-0295-5
16. T. Ahmad, K. Ahmad and M. Alam, *Procedia Environ. Sci.,* 35 (2016) 950. doi:10.1016/j.proenv.2016.07.099
17. E. C. Bernardo, R. Egashira and J. Kawasaki, *Carbon,* 35 (1997) 1217. doi:10.1016/S0008-6223(97)00105-X
18. V. Sygouni and C. V. Chrysikopoulos, *Chem. Eng. J.,* 262 (2015) 823. doi:10.1016/j.cej.2014.10.044
19. M.E. Fuziki, L. S. Ribas, A. M. Tusset, R. Brackmann, O. A. A. Dos Santos, and G. G. Lenzi, *Heliyon,* 9 (2023) e13678. doi:10.1016/j.heliyon.2023.e13678.
20. S. Ahmed, I. N. Unar, H. A. Khan Maitlo.G.,Mahar,R.B.,Jatoi,A.S.,Memon ,A.Q. and shah, A.K. *Environ. Sci. Pollut. Res.,* 27 (2020) 9619. doi:10.1007/s11356-019-07441-8
21. N. Boudechiche, N. Morante, D. Sannino, K. Monzillo, M. Trari and Z. Sadaoui, *Catalysts,* 14 (2024) 883. doi:10.3390/catal14120883
22. T. N. Rao, Riyazuddin, P. Babji, N. Ahmad, R. A. Khan, I. Hassan, S. A. Shahzad and F. M. Husain, *Saudi J. Biol. Sci.*, 26 (2019) 1385. doi:10.1016/j.sjbs.2019.09.005
23. O. Avciata, Y. Benli, S. Gorduk and O. Koyun, *J. Eng. Technol. Appl. Sci.,* 1 (2016) 34. doi:10.30931/jetas.281381
24. T. Ivanova, A. Harizanova, T. Koutzarova and B. Vertruye., *Opt. Mater.* 36 (2013) 207. doi:10.1016/j.optmat.2013.08.030
25. S. Abbad, K. Guergouri, S. Gazaout, S. Djebabra, A. Zertal, R. Barille and M. Zaabat, *J. Environ. Chem. Eng.,* 8 (2020) 103718. doi:10.1016/j.jece.2020.103718.
26. S. M. Al Amin and M. A. Kowser, *Heliyon,* 10 (2024) e37558. doi:10.1016/j.heliyon.2024.e37558
27. G. E. Putri, S. Arief, N. Jamarun, F. R. Gusti and A. N. Sary, *Orient. J. Chem.,* 34 (2018) 629. doi:10.13005/ojc/340629
28. L. A. G. Pohan, O. Kambiré, M. Nasir and L. Ouattara, *Modern Res. Catal.,* 9 (2020) 94004. doi:10.4236/mrc.2020.94004
29. C. Cao, C. Hu, X. Wang, S. Wang, Y. Tian and H. Zhang, *Sens. Actuators B Chem.,* 156 (2011) 114. doi:10.1016/j.snb.2011.03.023
30. R. Khan, N. Rahman, A. Prasannan, K. Ganiyeva, S. Chakrabortty and S. Sangaraju, *Sci. Rep.,* 15(1) (2025) 20309. doi:10.1038/s41598-025-07000-x.
31. H.-Y. Jung, I.-S. Yeo, T.-U. Kim, H.-C. Ki and H.-B. Gu, *Appl. Surf. Sci.,* 432 (2018) 266. doi:10.1016/j.apsusc.2017.09.217

32. M. N. Nawaz, Z. Zhang, W. Yuan and Khan, *S.B. Energy Nexus,* 19 (2025) 100495. doi:10.1016/j.nexus.2025.100495.
33. F. Septiningrum, A. H. Yuwono, F. A. Maulana, E. N. Nurhidayah, D. Dhaneswara, N. Sofyan, H. Hermansyah and W. W. Purwanto, *Curr. Res. Green Sustain. Chem.,* 8 (2024) 100394. doi:10.1016/j.crgsc.2023.100394
34. R. Ratshiedana, M. E. Malefane, O. J. SFakayode, G. K. More, A. K. Mishra and A. T. Kuvarega, *Mater. Today Commun.*, 41 (2024) 110753. doi:10.1016/j.mtcomm.2024.110753
35. C. H. Nguyen, H. N. Tran, C.-C. Fu, Y.-T. Lu and R.-S. Juang, *J. Taiwan Inst. Chem. Eng.,* 109 (2020) 51. doi:10.1016/j.jtice.2020.02.019
36. C. Sahoo, A. K. Gupta and I. M. S. Pillai, *J. Environ. Sci. Health, Part A*, 47 (2012) 1428. doi:10.1080/10934529.2012.672387S.
37. S. K. Sahu, A. Palai and D. Sahu, *Sustain. Chem. Environ*., 8 (2024) 100162. doi:10.1016/j.scenv.2024.100162
38. M. Delnavaz, S. Amiri and S. Najari, *Ecotoxicol. Environ. Saf.,* 295 (2025) 118175. doi:10.1016/j.ecoenv.2025.118175
39. U. Kumari, A. Mishra, H. Siddiqi and B. C. Meikap, *J. Clean. Prod*., 279 (2021) 123645. doi:10.1016/j.jclepro.2020.123645
40. D. Ramutshatsha-Makhwedzha, A. Munyengabe, M. L. Mavhungu, R. Mbaya and J. Baloyi, *Biomass Convers. Biorefin.,* 14 (2023) 21757. doi:10.1007/s13399-023-04329-z
41. T. Ali, A. Ahmed, U. Alam, I. Uddin, P. Tripathi and M. Muneer, *Mater. Chem. Phys*., 212 (2018) 325. doi:10.1016/j.matchemphys.2018.03.05
42. Y. Cao, H. Tan, T. Shi, T. Tang and J. Li, *J. Chem. Technol. Biotechnol*., 83 (2008) 546 doi:https://doi.org/10.1002/jctb.1831
43. S.B. Aziz, G. Hussein, M.A. Brza, S. J. Mohammed, R. T. Abdulwahid, S.R. Saeed and A. Hassanzadeh, *Nanomaterials*, 9 (2019) 1557. doi:10.3390/nano9111557.
44. Z. Wang, Z. Lv, Q. Su, X. Lai, Z. Huang, K. Li, L. Deng and J**.** Li, *Int. J. Biol. Macromol***.,** 266 (2024) 131013. doi:10.1016/j.ijbiomac.2024.131013.
45. W. Li, E. Yu-Yu, L.-Y. Cheng, M. Ding, Li, W.-Y. Diao, K.-S. Liu, S.-G. Li, K. Lu, H.-Q. F.-H. Lei, and J.-X. Jiang, *LWT*, 132 (2020) 109937. doi:10.1016/j.lwt.2020.109937.
46. S. Rizvi, A. Singh and S. K. A. Gupta, *Appl. Water Sci.,* 12 (2022) 81. doi:10.1007/s13201-022-01620-8.
47. B. O. Otieno, S. O. Apollo, B. E. Naidooand A. Ochieng, *J. Environ. Sci. Health Part A,* 52 (2017) 616. doi:10.1080/10934529.2017.1294963.